Role of Non-Temperature-Gradient Power Flow Terms in Low-Temperature Regenerators

R. Snodgrass, J. Ullom, and S. Backhaus

National Institute of Standards and Technology, Boulder, CO 80305
Department of Physics, University of Colorado Boulder, Boulder, CO 80309

ABSTRACT

The total power flow through cryocooler regenerators is key to their performance because it reduces the cooling available at the cold heat exchanger. At temperatures near 4 K, the real-fluid properties of helium and the finite heat capacity of regenerator matrix solids are responsible for large components of total power flow that depend upon temperature but not upon temperature gradient. Near the warm end of 4 K cryocooler regenerators, non-temperature-gradient power flow terms are small, and total power flow in regenerators is conserved by terms that are proportional to the temperature gradient. In this work, we combine analytics with experiment to show that the qualitative shape of the temperature profile in low-temperature regenerators is determined by the relative size of the non-temperature-gradient power flow terms at the warm and cold ends. In most 4 K regenerators, the temperature profile is flat at the cold end and the temperature gradient is large near the warm end; however, because the real-fluid and finite-heat-capacity power flow terms vary so rapidly with temperature, relatively small increases to the cold-end temperature above 4 K may result in an abrupt transition of the temperature profile, becoming flat at the warm end with large temperature gradient at the cold end. If this transition occurs, the cooling available at the cold heat exchanger is actually determined by fluid and material properties at the warm end. We use the abrupt transition between these two profiles as a probe to determine when the non-temperature-gradient power flow terms are equivalent at the two ends of the regenerator, and present analytics to predict when (or if) the transition may occur. Regenerators made with gadolinium oxysulfide at the cold end are not likely to experience the abrupt transition in temperature profile, while holmium copper regenerators should exhibit the transition at cold-end temperatures near 7 K.

INTRODUCTION

Two-stage, low-frequency (~ 1 Hz) pulse tube refrigerators or Gifford-McMahon cryocoolers are commonly used to reach temperatures near 4 K from room temperature. It is critical to understand total power flow through the regenerators of these refrigerators because this quantity significantly reduces the cooling power available at the cold heat exchangers. Power flow through the first stage regenerator is usually small relative to the acoustic power flow because helium can be treated as an ideal gas and regenerator matrix materials have sufficient heat capacity at such temperatures (first-stage regenerators do not usually cool to much below 40 K).

The situation in the second-stage regenerator is very different from the first. Below about 20 K, power flows from real-fluid effects and finite-heat-capacity effects may be very large and

vary rapidly as a function of temperature (these terms will be calculated and shown later in this manuscript). Near 4 K, the power flow through the regenerator is effectively set by the temperature of the cold end, the material and geometry of the regenerator matrix, and the acoustic power flow. Broadly speaking, behavior of the regenerator at these temperatures can be understood by analyzing power flow terms that depend upon temperature but not upon the temperature gradient.

The large, non-temperature-gradient power flow terms are responsible for much of the unique behavior in 4 K cryocooler regenerators. A large amount of heat (a few watts) can typically be intercepted along the regenerator of 4 K cryocoolers with little-to-no effect on the cooling available at the cold end. Additionally – as we will discuss in this work – the qualitative shape of the temperature profile can vary drastically by making only small changes to the temperature of the cold end. Under some conditions, it is possible that the cooling available at the cold end of the second stage is determined by material and fluid properties not at the cold end but at the warm end.

Total power flow $\dot{H}_2$ subtracts from cold-end cooling power

We have previously [1] shown that total power flow directly subtracts from the cooling available at the cold heat exchanger; the following paragraph is a summary explaining the same. Consider a First Law box that completely encompasses the second-stage heat exchanger, including very small amounts of the regenerator and thermal buffer tube. The powers flowing into the box are the cooling power $\dot{Q}_c$ and the total power flow at the cold end of the second-stage regenerator $\dot{H}_{2,c}$. If no heat is applied to the regenerator along its length and it is well insulated, the total power flow at the cold end of the regenerator is equal to the total power flow everywhere in the regenerator, i.e., $\dot{H}_{2,c} = \dot{H}_2(x) = \dot{H}_2$, where x is the longitudinal axis of the regenerator. The power flowing out of the First Law box is the total power flowing into the second-stage thermal buffer tube. This power is equal to the acoustic power flow at the cold end of the second-stage buffer tube $\dot{E}_{2,c}$ (as the hydraulic radius of the buffer tube is much larger than the thermal penetration depth) plus any enthalpy carried by steady flow. The gross cooling power is then

$$\dot{Q}_c = \dot{E}_{2,c} + \dot{N}h_c - \dot{H}_2, \tag{1}$$

where $\dot{N}$ is the steady molar flow rate and h_c is the molar enthalpy of helium at the cold-end temperature. Equation (1) shows that the total power flow directly subtracts from the cooling power and that the maximum cooling power is[1] $\dot{E}_{2,c}$ if total power flow is 0.

The equation for total power flow $\dot{H}_2$

We have previously developed analytics for approximating the total power flow through cryocooler regenerators. These approximations were made by beginning with the thermoacoustic framework pioneered by Rott [2] and Swift [3], and are only valid if the hydraulic radius of the regenerator's matrix material is small compared to the thermal penetration depth [4] (which is true for the regenerator discussed in this work). The total power flow $\dot{H}_2$ through the regenerator can be approximated as

$$\begin{aligned}\dot{H}_2(x) \approx (1 - T_m\beta)\dot{E}_2 + \left(\frac{\varepsilon_s}{1+\varepsilon_s}\right)T_m\beta\dot{E}_2 + \dot{N}h \\ +F(x,T_m)|U_1|^2\frac{dT_m}{dx} - \left(A_g k + A_s k_s\right)\frac{dT_m}{dx},\end{aligned} \tag{2}$$

which is also written in short-hand as

$$\dot{H}_2(x) \approx \dot{H}_\beta + \dot{H}_\varepsilon + \dot{H}_m + \dot{H}_{\nabla T} + \dot{H}_\kappa. \tag{3}$$

[1] The power flow due to streaming or steady flow does not affect the cooling power at the cold end because $\dot{N}h_c$ is also contained in $\dot{H}_2$ (i.e., this term is equivalent at the cold end of the second-stage regenerator and buffer tube).

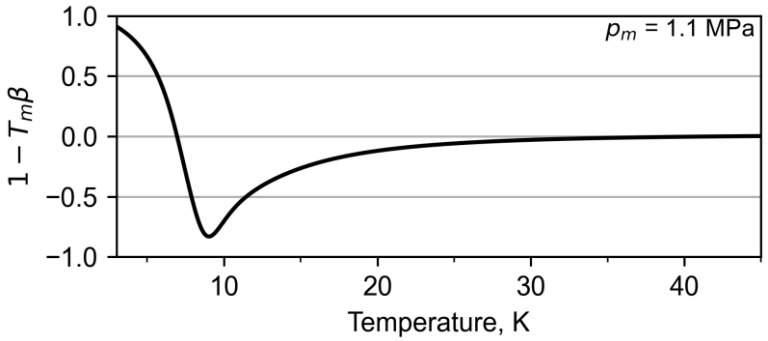

Figure 1. One minus the mean temperature multiplied by the thermal expansion coefficient. Fluid properties for ^{4}He were calculated at a mean pressure p_m of 1.1 MPa.

We will now proceed to discuss each term of the total power flow equation. The first two terms of Eqs. (2) and (3) scale by the acoustic power flow $\dot{E}_2 = \mathrm{Re}[p_1\widetilde{U_1}]/2$. Acoustic power may be known more colloquially as "PV" power. The subscript in $\dot{E}_2$ shows that acoustic power is the product of two terms that are first-order in size: p_1 the pressure oscillation phasor and $\widetilde{U_1}$ the complex conjugate of the volume flow rate phasor. The mean temperature T_m of the regenerator is a function of x, and the thermal expansion coefficient $\beta \equiv -\frac{1}{\rho}\frac{\partial\rho}{\partial T}\Big|_p$ is a strong function of T_m. The density of the gas is ρ.

The product $T_m\beta$ is nearly equal to 1 at temperatures above about 40 K (Fig. 1), so that the real-fluid power flow term $\dot{H}_\beta$ is small in first-stage regenerators or at the warm end of second-stage regenerators; however, as we will show later in this manuscript, the $\dot{H}_\beta$ term should not be completely ignored when analyzing small changes to total power flow, as $\dot{E}_2$ can be relatively large at the warm end of the second-stage regenerator. For ^{4}He at 1.1 MPa and a mean temperature of 3 K, the real-fluid contribution $\dot{H}_\beta$ is very large at about $0.91\dot{E}_2$. From Eq. (1), we see that at 3 K 91% of the available cooling power is lost to real-fluid effects alone.

The second term $\dot{H}_\varepsilon$ is the power flow resulting from the finite heat capacity of the regenerator material. The ratio of the fluid to solid volumetric heat capacities in the regenerator is $\varepsilon_s = \phi\rho c_p/(1-\phi)\rho_s c_s$, where ϕ, ρ_s, c_s are porosity, solid density, and solid specific heat, respectively. Like $\dot{H}_\beta$, this power flow term is very sensitive to T_m near 4 K through dependence upon $T_m\beta$. Because materials commonly used in these regenerators have distinct heat capacities that vary dramatically at low temperatures, $\dot{H}_\varepsilon$ is highly material dependent. Later in this manuscript, we will show how different regenerator materials can lead to large differences in the qualitative behavior of the regenerator temperature profile.

The third term $\dot{H}_m$ is the last that is not dependent upon the temperature gradient. It is the power flow due to streaming or steady mass flow, known more colloquially as "DC" flow. In the 4 K regenerator studied in this work, $\dot{H}_m$ is an appreciable component of $\dot{H}_2$ at the warm end (where $h - h_c$ is significant) but not at the cold end (where $h - h_c$ is zero). In a previous work, we showed that $\dot{N}$ may be estimated by applying heat to the regenerator and measuring the response of the temperature profile [1].

The fourth and fifth terms in Eqs. (2) and (3) ($\dot{H}_{\nabla T}$ and $\dot{H}_\kappa$) only contribute to power flow at locations in the regenerator with non-zero temperature gradient. The $F(x, T_m)$ parameter in $\dot{H}_{\nabla T}$ is defined in [1]. The fifth term, $\dot{H}_\kappa$, is thermal conduction. The thermal conductivities of the gas and solid are k and k_s, respectively, while the effective cross-sectional areas of each are A_g and A_s.

The two terms containing dT_m/dx will not be discussed at a deeper level in this work. Instead, we will focus on the non-temperature-gradient terms. Because these terms explain so much about regenerator behavior, we give the sum of these terms its own name:

$$\dot{H}_0(T_m) \equiv \dot{H}_\beta + \dot{H}_\varepsilon + \dot{H}_m. \tag{4}$$

EXPERIMENTAL METHODS

The following is a summary of our experimental methods; please see our related publications for more details [1], [4]–[6]. All experiments were conducted using a two-stage, commercial pulse tube refrigerator operating at 1.4 Hz. The no-load temperature of the second stage is about 2.3 K.

The second-stage regenerator was highly instrumented with a large number of copper split clamps that fit snugly around the regenerator. About 21 pairs of split clamps were fastened to the regenerator (using stainless steel screws): 10 were capable of injecting heat into the regenerator (this capability was not used in this study), and 11 were used to measure the temperature profile of the regenerator. This resulted in a spatial measurement resolution of about 1.5 cm. In some experiments, the temperature on each half of the split clamps was measured, so that temperature profiles could be built for two sides of the regenerator (azimuthal temperature variation was measured). Calibrated silicon diode thermometers were used to measure the temperature along the regenerator and to measure the temperature of the warm T_w and cold T_c heat exchangers. We measured no significant change to the cooling power available at the cold and warm heat exchangers with and without the split clamps attached to the regenerator, and therefore trust they do not significantly affect the cryocooler's behavior [4].

Temperature profiles are reported as functions of x/L, where x is the distance along the longitudinal axis of the regenerator starting at the warm end. The length of the regenerator is L, so that the warm and cold ends are located at x/L = 0 and 1, respectively. All temperature profiles are shown in steady state, and all temperatures were calculated by commercial temperature monitors (time-averaged values are reported). Heaters were placed on the warm and cold heat exchangers so that the temperature of the warm and cold ends could be regulated to a variety of temperatures.

RESULTS AND ANALYSIS

Qualitative shape of the temperature profile

In this section, we qualitatively discuss the shape of temperature profiles in 4 K cryocooler regenerators. Figure 2 shows (generally) the variety of shapes we have observed during our experiments on the pulse tube refrigerator discussed here. The profiles shown in Fig. 2 arise simply by regulating the cold end to slightly different temperatures.

Let us proceed by analyzing each of the plotted profiles. We begin with the profile labeled as *normal*, which was measured while regulating the cold end to 2.3 K. This profile is considered normal because in most cases these cryocoolers are operated at cold-end temperatures near and below 4 K. Figure 2 shows that almost all of the temperature change between T_w and T_c is concentrated near the warm end, while the last third of the regenerator has nearly zero temperature gradient. Because dT_m/dx = 0 at the cold end, the total power flow there is equal to $\dot{H}_0$, and because no heat was applied to the regenerator, we conclude that $\dot{H}_2 \approx \dot{H}_{0,c}$ (the subscript c denotes evaluation at T_c). The cold end is at or near[2] the minimum temperature of the regenerator, so steady flow carries no enthalpy here when compared to warmer parts of the regenerator, and $\dot{H}_2 \approx \dot{H}_{0,c} = \dot{H}_{\beta,c} + \dot{H}_{\varepsilon,c}$. From Eq. (2) we can conclude that the total power flow everywhere in the regenerator is set by the temperature, the regenerator matrix material, and the acoustic power flow at the cold end. As we will show later in the manuscript, it is mostly the real-fluid power flow term that dominates total power flow at this temperature.

[2] As shown in [4], portions of the regenerator near the cold end may be slightly colder than the cold heat exchanger.

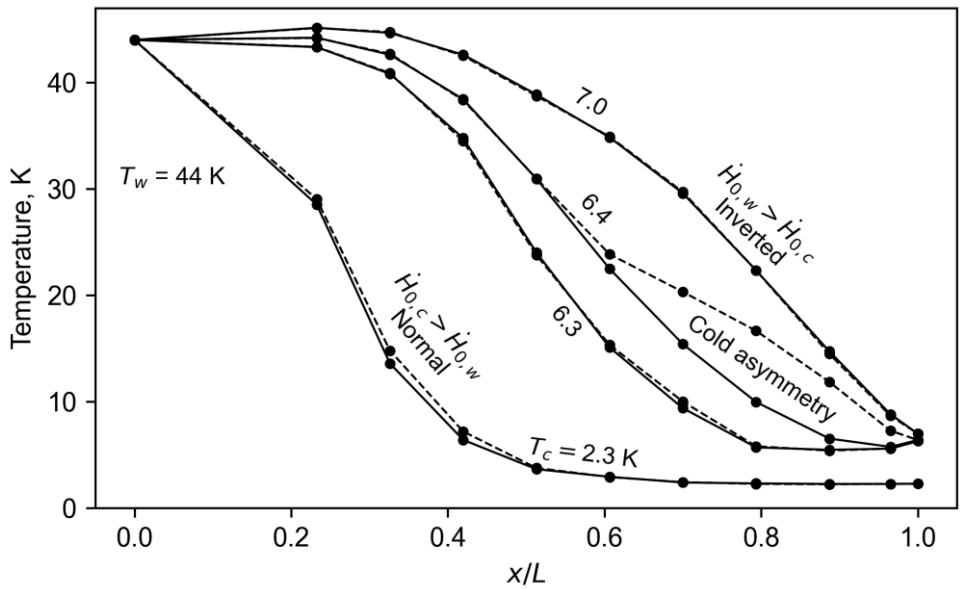

Figure 2. The qualitative shape of the temperature profile can vary widely with small changes to cold-end temperature T_c. The warm-end temperature T_w was regulated to 44 K for all profiles. The solid and dashed lines are opposite sides of the same profile (i.e., a measurement of azimuthal variation).

At the warm end of the normal profile there exists a negative temperature gradient. For $dT_m/dx < 0$, $\dot{H}_{\nabla T} + \dot{H}_\kappa$ carry positive amounts of power [4]. This requires $\dot{H}_{0,w} < \dot{H}_{0,c}$, as total power flow is conserved through the regenerator ($d\dot{H}_2/dx = 0$). In fact, everywhere in the regenerator the temperature gradient adjusts so that $\dot{H}_{\nabla T} + \dot{H}_\kappa = \dot{H}_{0,c} - \dot{H}_0$. The temperature gradient provides the pliability of the system. Although $\dot{H}_0$ varies widely between T_w and T_c and is set by parameters of the system (materials, geometry, supplied acoustic power), a flexible temperature gradient is necessary to conserve total power flow. Any location in the regenerator where $dT_m/dx = 0$ can be thought of as fixing the total power flow through the regenerator, as $\dot{H}_2$ must equal $\dot{H}_0$ there.

Now consider the profile labeled *inverted*, which was measured while regulating the cold end to 7.0 K. In this profile dT_m/dx is large and negative at the cold end and nearly zero at the warm end. The situation is opposite from the normal profile previously described: since there is no gradient at the warm end, we conclude that $\dot{H}_2 \approx \dot{H}_{0,w}$ and $\dot{H}_{0,c} < \dot{H}_{0,w}$. This transition from normal to inverted over such a small change in one end condition (T_c from 2.3 K to 7 K) is a remarkable demonstration of how greatly the real-fluid (as seen in Fig. 1) and finite-heat-capacity power flow terms vary at low temperatures.

Figure 2 also shows two other profiles that occur near the transition from normal to inverted. The profile shown for T_c = 6.3 K has nearly zero temperature gradient at both the warm and cold ends[3]. Following from our previous discussion, it is then true that $\dot{H}_2 \approx \dot{H}_{0,w} \approx \dot{H}_{0,c}$. Increasing the cold-end temperature by just 0.1 K produces a profile labeled *cold asymmetry*. In a section nearest its cold end, one half of the regenerator is warmer than the other, and azimuthal temperature differences of up to 7 K are observed. More details on temperature asymmetries in this regenerator are given in [5]. As we will show in the following sections, the cold-end temperature asymmetry seems to occur near the condition $\dot{H}_{0,w} \approx \dot{H}_{0,c}$.

Acoustic power scaling for regenerators with small hydraulic radius

Calculations for $\dot{H}_0$ at the warm and cold ends of the regenerator are central to the analysis presented in this manuscript. In this section, we provide details on how acoustic power scales through the regenerator – a necessary preliminary result because two of the three components in $\dot{H}_0$ are proportional to $\dot{E}_2$.

[3] As discussed in [1], this provides a method for measuring steady flow through the regenerator ($\dot{N}$). If acoustic power is known or may be estimated and the materials in the regenerator are known, setting $\dot{H}_{0,c} = \dot{H}_{0,w}$ gives $\dot{N}$.

In our previous works [1], [4] we gave a methodology for estimating acoustic power at the cold end of the regenerator $\dot{E}_{2,c}$. To find total power flow at the warm end, however, it is necessary to understand how $\dot{E}_2$ varies through the regenerator. The thermoacoustic framework [7] tells us that the gradient of the acoustic power is

$$\frac{d\dot{E}_2}{dx} = -\frac{r_v}{2}|U_1|^2 - \frac{1}{2r_\kappa}|p_1|^2 + \frac{1}{2}\mathrm{Re}[g\widetilde{p_1}U_1]. \tag{5}$$

In Eq. (5), the first and second terms on the right-hand side represent viscous dissipation and thermal relaxation effects, respectively. The viscous resistance per unit length is r_v and $1/r_\kappa$ is the thermal-relaxation conductance per unit length. For a regenerator with small hydraulic radius (compared to viscous and thermal penetration depths) both of these terms are very small. This is true for the low-frequency regenerator analyzed here, and therefore the first two terms of Eq. (5) can be neglected. Acoustic power then changes through the regenerator due only to the third term on the right-hand side, which is referred to as the gain term. The gain g is equal[4] to $\beta/[1+\varepsilon_s(T_m,x)]dT_m/dx$ for the regenerator of interest here, so Eq. (5) can be re-written as

$$\frac{1}{\dot{E}_2}\frac{d\dot{E}_2}{dx} \approx \frac{\beta}{1+\varepsilon_s(T_m,x)}\frac{dT_m}{dx}. \tag{6}$$

Integrating between T_c and T_w, we find

$$\frac{\dot{E}_{2,w}}{\dot{E}_{2,c}} \approx \exp\left[\int_{T_c}^{T_w}\frac{\beta}{1+\varepsilon_s(T_m,x)}\,dT_m\right]. \tag{7}$$

In the above, ε_s is written as $\varepsilon_s(T_m,x)$ to emphasize that the heat capacity of the regenerator may be discontinuous at the transitions between matrix materials, so knowledge of the complete temperature profile may be needed to evaluate the above integral. For a single-material regenerator or a regenerator with the majority of the temperature span isolated to a single-material, $\varepsilon_s(T_m,x) \sim \varepsilon_s(T_m)$ and $\dot{E}_{2,w}$ can be evaluated without knowledge of $T_m(x)$ but only with the cold-end and warm-end temperatures. This is approximately true for a temperature profile that is very near the transition between normal and inverted (e.g., Fig. 2 for T_c = 6.3 K), where the temperature span is mostly contained to the material in the middle of the regenerator. In the next section, our analysis will focus on the transition between normal and inverted, so we calculate $\dot{E}_{2,w}$ by approximating $\varepsilon_s(T_m,x)$ using the properties of the middle regenerator material, which is Er_3Ni. Equation (7) is then easily evaluated for any T_c and T_w.

For a regenerator with infinite heat capacity the exponential of the integral in Eq. (7) simplifies to ρ_c/ρ_w, and for a regenerator with infinite heat capacity operating in the ideal gas regime it simplifies to T_w/T_c. However, these simplifications are generally not appropriate for this study.

Using $\dot{H}_0$ to predict the shape of the temperature profile

The qualitative discussion of the temperature profiles shown in Fig. 2 will now be verified by comparing calculations of $\dot{H}_{0,w} = \dot{H}_{0,c}$ against experimental observation of the temperature asymmetry.

The top half of Fig. 3 gives calculations for $\dot{H}_0$ at the cold end (subplot a) and warm end (subplot b) using Eq. (2). All calculations are normalized by $\dot{E}_{2,c}$, emphasizing that the shape of the profile is not directly dependent upon the acoustic power at the cold end. Fluid properties were

[4] This is the same result presented by Swift [7] except that real-fluid and finite-heat-capacity effects are accounted for. The most-general form of g is recorded in the continuity equation in [8], but for small hydraulic radius it can be simplified to $\beta/[1+\varepsilon_s(T_m,x)]dT_m/dx$.

calculated at a mean pressure p_m of 0.99 MPa because experiments were performed at about the same pressure. To calculate $\dot{H}_\varepsilon$, we assumed a packed sphere matrix with porosity ϕ = 0.39.

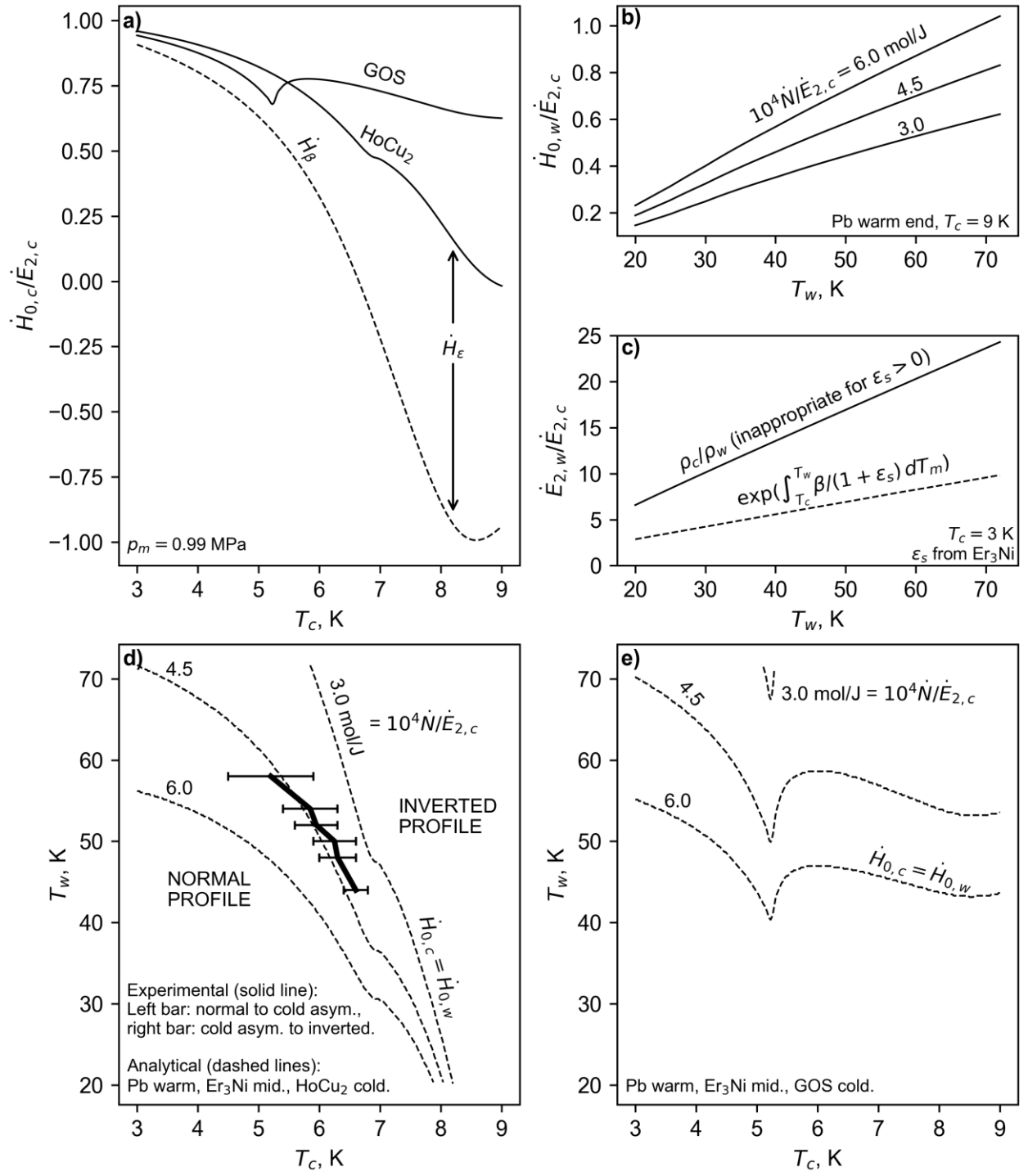

Figure 3. Calculated values for $\dot{H}_0$ at a) cold-end temperatures and b) warm-end temperatures. The non-temperature-gradient power flow term $\dot{H}_0$ is normalized by the acoustic power at the cold end. In a) the solid lines give $\dot{H}_{0,c}$ for two different cold-end materials, while the dashed line shows the power flow component due to real-fluid effects. At the warm end, b) shows $\dot{H}_0$ growing with increasing steady flow rate and with increasing T_w (due to the increase in $\dot{E}_{2,w}$). Our best estimate for $10^4\dot{N}/\dot{E}_{2,c}$ is 6.0 mol/J for the pulse tube refrigerator studied here. Subplot c) plots the ratio of acoustic power at the warm end to that at the cold end. For a regenerator with finite heat capacity, the ratio of densities cannot be used and instead ε_s must be accounted for using Eq. (7) (see text for details). The dashed lines in subplots d) and e) show the temperatures where $\dot{H}_{0,c} = \dot{H}_{0,w}$ for Pb-Er_3Ni-$HoCu_2$ and Pb-Er_3Ni-GOS regenerators, respectively. Above the dashed lines the profile should be inverted, while below the lines the profile should be normal. The thick line with error bars in d) shows the measured temperature range over which a temperature asymmetry was present at the cold end, similar to the asymmetry shown in Fig. 2.

At the cold end, $\dot{H}_0$ is determined by real-fluid effects and finite-heat-capacity effects. The real-fluid contribution to power flow varies widely with temperature: at 3 K and 0.99 MPa it is $0.91\dot{E}_{2,c}$ while at 9 K it is $-0.94\dot{E}_{2,c}$. The heat capacity term was calculated for two materials commonly used at the cold end of these regenerators: $HoCu_2$ and GOS (gadolinium oxysulfide). Figure 3a shows that $\dot{H}_{0,c}$ varies strongly between these two materials. For a cold-end temperature of 8 K, $\dot{H}_{0,c}$ for GOS is about $0.7\dot{E}_{2,c}$, while for $HoCu_2$ it is $0.2\dot{E}_{2,c}$. This is a result of the very small heat capacity of GOS at temperatures above about 5.5 K [9]. For a material like $HoCu_2$, $\dot{H}_{0,c}$ decreases rapidly at temperatures above about 4 K as real-fluid power flow decreases, but for GOS $\dot{H}_{0,c}$ stays large because finite-heat-capacity power flow increases as real-fluid power flow decreases. The consequence of this is that the temperature profile of GOS regenerators is much less likely to invert, as we will soon show.

The non-temperature-gradient power flow terms at the warm end of the regenerator are plotted in Fig. 3b. These power flows are also normalized by $\dot{E}_{2,c}$, although they must be calculated using $\dot{E}_{2,w}$. Equation (7) was used to calculate $\dot{E}_{2,w}$ and is plotted as the dashed line in Fig. 3c. The ratio of the cold-end density to the warm-end density is also plotted in Fig. 3c, showing that acoustic power at the warm end would be overestimated by more than a factor of two if the finite heat capacity of the regenerator were not accounted for. Acoustic power at the warm end increases with increasing T_w or decreasing T_c.

Figure 3b also shows that higher amounts of streaming ("DC" flow) from the warm end towards the cold end increase $\dot{H}_{0,w}$. Therefore, streaming promotes an inverted profile and decreases the temperature gradient at the warm end. Finite-heat-capacity power flow in this figure was calculated assuming a warm end consisting of a packed Pb sphere bed with 0.39 porosity.

Figures 3d and 3e are maps predicting at what T_w and T_c combinations the regenerator's temperature profile should be normal or inverted. Figure 3d is for a regenerator with Pb at the warm end, Er_3Ni in the middle, and $HoCu_2$ at the cold end, while Fig. 3e is for the same regenerator but with GOS at the cold end[5]. In both figures, the dashed lines are temperature combinations where $\dot{H}_{0,w} = \dot{H}_{0,c}$. Above the dashed line, $\dot{H}_{0,w} > \dot{H}_{0,c}$ and the profile should be inverted; below the dashed line, $\dot{H}_{0,c} > \dot{H}_{0,w}$ and the profile should be normal. The three dashed lines show the influence of streaming on the inversion condition: lower amounts of streaming decrease the parameter space for which a temperature profile should be inverted. The amount of streaming and the acoustic power at the cold end has been estimated[6] in our previous works [1], [4]; however, there is some uncertainty on these quantities, so we have also plotted the result for our best-estimate of $\dot{N}/\dot{E}_{2,c}$ multiplied by factors of 0.75 and 0.5.

For the Pb-Er_3Ni-$HoCu_2$ regenerator the $\dot{H}_{0,w} = \dot{H}_{0,c}$ calculation suggests profile inversion will occur at any reasonable warm-end temperature once the cold-end temperature is above about 8 K. This is true for all three steady flow rates considered. The inevitability of profile inversion at higher T_c is a result of $HoCu_2$'s sufficient heat capacity at relatively high cold-end temperatures, which results in low $\dot{H}_{0,c}$ once the real-fluid contribution to total power flow becomes small or negative.

Now we compare our calculations for $\dot{H}_{0,w} = \dot{H}_{0,c}$ to the experimentally observed cold-end asymmetry, which is also plotted in Fig. 3d. We have contacted the manufacturer of this pulse tube refrigerator and do know that the regenerator materials agree with those we assumed in the

[5] In this work, inversion is predicted by only comparing power flows at the warm and cold ends; however, this regenerator is built from three materials, so inversion can be influenced by the middle material. The two-material (warm and cold ends only) simplified analysis is still relevant because it builds understanding of the non-temperature-gradient power flows and their influence on the shape of the temperature profile. Furthermore, we know that the heat capacity of the warm-end material is similar to the heat capacity of the middle material at warm-end temperatures, so treating the warm and middle materials as one should be appropriate when calculating the condition for temperature profile inversion.

[6] For mean pressure p_m = 0.99 MPa, $\dot{E}_{2,c}$ is estimated as 6.8 W. The steady molar flow rate $\dot{N}$ was estimated to be about 0.8 mmol/s in [1] before Eq. (7) was developed; however, using Eq. (7) to find $\dot{E}_{2,w}$ we update our estimate for $\dot{N}$ as 4.1 mmol/s.

calculations. The warm-end temperature was regulated to six different values between[7] 44 K and 58 K while the cold end was increased in temperature by 0.1 K increments. For all T_w, the temperature profiles began as normal and eventually changed to inverted. The thickest line in Fig. 3d shows the mean T_c value between when the temperature asymmetry first developed and when it disappeared (i.e., when the profile was fully inverted). As we showed in Fig. 2, the cold-end asymmetry occurs close to the condition when $\dot{H}_{0,w} = \dot{H}_{0,c}$. That the measured temperature asymmetry occurs very close to the calculated inversion condition (when allowing for a 25% error in the estimate of $\dot{N}/\dot{E}_{2,c}$) gives credibility to our hypothesis that $\dot{H}_0$ determines the qualitative shape of the temperature profile and to the relatively simple approximations for $\dot{H}_\beta$ and $\dot{H}_\varepsilon$ given in Eq. (2).

The lines of $\dot{H}_{0,w} = \dot{H}_{0,c}$ for a Pb-Er_3Ni-GOS regenerator (Fig. 3e) are much different. Depending on the ratio of $\dot{N}/\dot{E}_{2,c}$, many warm-end temperatures cannot result in an inverted profile, no matter how high T_c is. This result is consistent with our experimental observations. We have multiple 4 K cryocoolers which have never displayed temperature profile inversion, even at elevated T_c. Based on the shape of the cooling capacity maps for these pulse tubes, we find it likely that GOS is the material at the cold end of the regenerators. We have also studied regenerator cooling in a two-stage Gifford-McMahon cryocooler and found that the regenerator's temperature profile would not invert at very high T_c [10], also suggesting that its regenerator is built with GOS.

Warm-end properties determine cold-end cooling if $dT_w/dx \approx 0$

It has been well documented [1], [4], [6], [10]–[12] that 4 K cryocoolers can provide cooling not only at the cold heat exchanger but also along the regenerator. Applying heat to the regenerator usually has little effect on the cooling available at the cold end. This is possible because $\dot{H}_2 = \dot{H}_{0,c}$ and heat applied to the regenerator is accommodated by a decrease to the magnitude of the temperature gradient near the warm end and a decrease in power flow at locations upstream of heat injection (i.e., toward the warm end) due to the temperature gradient terms in Eq. (2). Essentially, regenerator cooling is possible in a normal profile because performance of the regenerator is set only by conditions at the cold end. For an inverted profile ($\dot{H}_2 \approx \dot{H}_{0,w}$), the opposite should be true and the warm end should determine cold-end cooling power.

The cold end of the pulse tube refrigerator described here was regulated to 20 K while sweeping T_w between 45 K and 65 K (Fig. 4a). All of the resulting profiles were inverted with nearly zero temperature gradient at the warm end. Under these conditions, we can estimate $\dot{H}_2 \approx \dot{H}_{0,w}$ for all profiles. Each component of $\dot{H}_{0,w}$ was calculated using Eq. (2) and is plotted in Fig. 4b.

There was extra complexity in calculating $\dot{E}_{2,w}$ for the data from this experiment. In [4] we showed that $\dot{E}_{2,c}$ is proportional to ${p_1}^2$, which can vary with the mean pressure of the compressor or with large changes to the temperature profile. The pressure oscillation in this experiment was measured using the electronic pressure gauges on the inlet and outlet of the pulse tube compressor. The term $(p_1/p_{1,45K})^2$ is plotted in Fig. 4c, showing that the square of the pressure oscillation for T_w = 65 K is 17% higher than for T_w = 45 K. In [4] $\dot{E}_{2,c}$ was estimated as 9.1 W when p_1 was 0.64 MPa, so we estimated $\dot{E}_{2,c} \approx 9.1\ \text{W} \left(\frac{p_1}{0.64\ \text{MPa}}\right)^2$. To calculate $\dot{E}_{2,w}$, we then used the acoustic power scaling given by Eq. (7), which is plotted in Fig. 4d.

As plotted in Fig. 4b, the change[8] in $\dot{H}_{0,w}$ as T_w increased from 45 K to 65 K was calculated as +2.3 W. Because $\dot{H}_2$ is determined by $\dot{H}_{0,w}$ for these inverted profiles, we would then expect a

[7] At higher warm-end temperatures the cold end could not be regulated low enough to produce a normal profile. For example, when T_w = 62 K, the cold-end asymmetry persisted between T_c = 3.6 K (the no-load temperature) and T_c = 4.9 K.

[8] Interestingly, the real-fluid contribution $\dot{H}_\beta$ is not insignificant from 45 K to 65 K – a consequence of large $\dot{E}_{2,w}$: even though $1 - T_m\beta$ is 0.016 at 65 K, $\dot{E}_{2,w}$ is about 39 W.

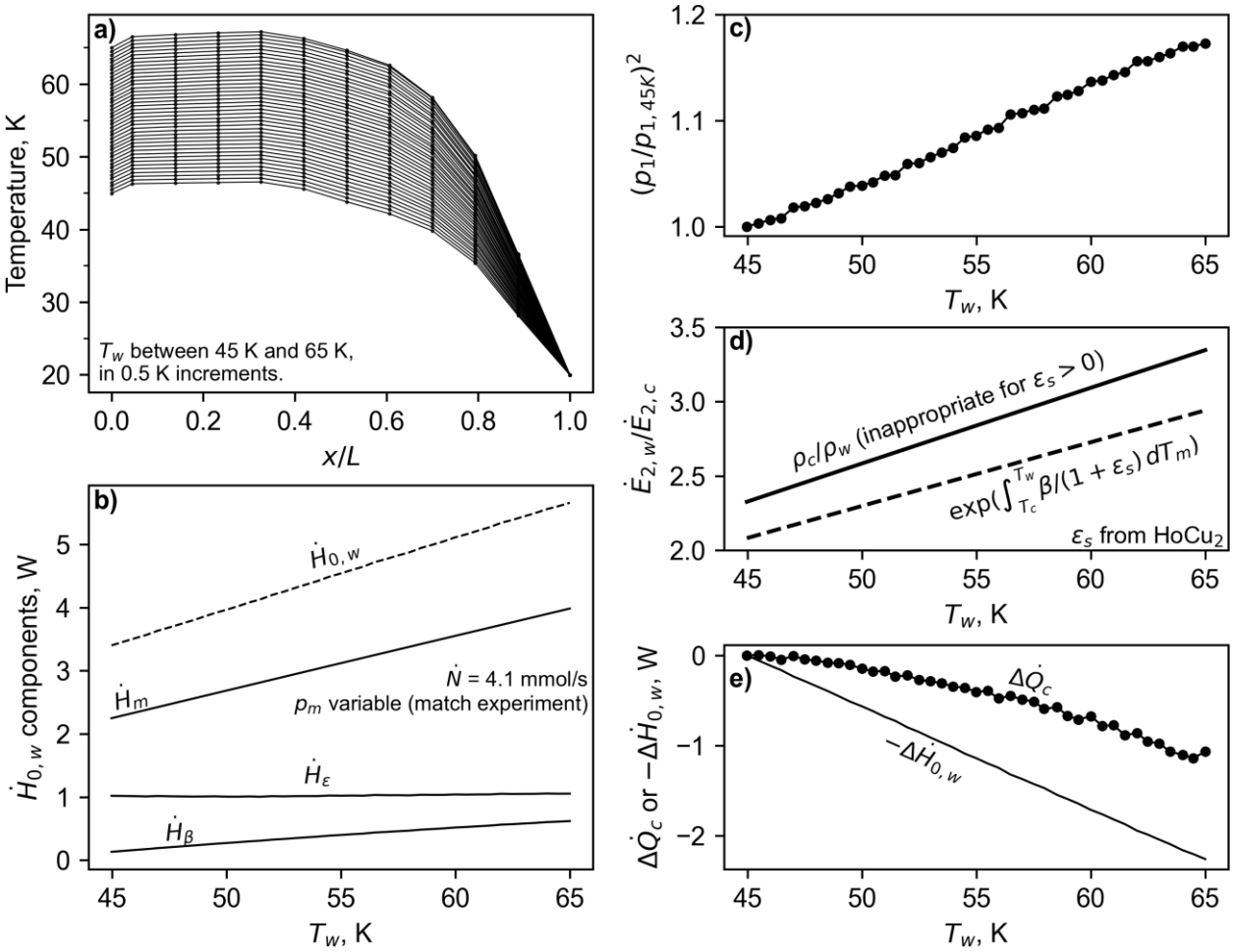

Figure 4. An experimental demonstration of the warm end determining cold-end cooling power. a) Steady-state temperature profiles when T_w was regulated between 45 K and 65 K, while T_c was held at 20 K. b) Non-temperature-gradient power flow terms calculated using Eq. (2). Please see the text for details on how acoustic power at the warm end was calculated. c) The pressure oscillation normalized by the pressure oscillation at 45 K, squared. d) Acoustic power scaling as calculated by Eq. (7) (dashed line) with the density ratio (solid line) for comparison. The density ratio gives a fair estimate here because ε_s is small at these temperatures. The exponential of the integral in Eq. (7) was calculated assuming all the temperature change occurs in the coldest regenerator material, which is $HoCu_2$. e) The measured change in cooling power at 20 K as T_w was increased to 65 K. Also plotted is the calculated change in non-temperature-gradient power flow terms at the warm end multiplied by −1.

decrease to the cold-end cooling power of 2.3 W; however, the cool-end cooling power was measured to decrease by only 1.1 W (Fig. 4e). We suspect that our calculation for $-\Delta\dot{H}_{0,w}$ does not match the measured $\Delta\dot{Q}_c$ because of an inaccurate estimate for $\dot{N}$ under these operating conditions. This parameter was calculated [1] using a temperature profile where the cold end was regulated to 3 K, which is much different from the profiles shown in Fig. 4a (where the cold end was regulated to 20 K). More work is necessary to characterize how steady flow through the regenerator may change between such vastly different temperature profiles.

CONCLUSION

In this work we have demonstrated the importance of the non-temperature-gradient power flow terms, the sum of which we call $\dot{H}_0$. The performance of low-temperature regenerators can generally be understood by considering only $\dot{H}_0$. For example, in most regenerators operating near 4 K, the total power flow through the regenerator and therefore the cooling available at the cold end will be determined exclusively by the power flow terms related to real-fluid and finite-heat-capacity effects. For a regenerator with sufficiently small hydraulic radius, the equation for $\dot{H}_0$ is relatively simple, making it an extremely powerful analytical tool. The validity of our simplified

equation for $\dot{H}_0$ (Eqs. (2) and (4)) has been bolstered through the experimental result shown in Fig. 3d, as well those in our other studies [1], [4].

The cold end of most 4 K regenerators should have nearly zero temperature gradient because real-fluid effects are large and approach the size of the acoustic power flow. In other parts of the 4 K regenerator – especially at the warm end – non-temperature-gradient power flow terms are smaller, so the temperature gradient must adjust to conserve total power. If the cold end of the regenerator is regulated to higher temperatures, e.g., above 7 K, real-fluid effects no longer dominate. For regenerator materials such as $HoCu_2$ (with large heat capacity over a wide temperature range), $\dot{H}_0$ at the cold end can then become smaller than that at the warm end, and the profile can become inverted. In an inverted profile, the temperature gradient is located at the cold end and the warm end shows nearly zero gradient. For a regenerator material such as GOS (with small heat capacity above about 5.5 K), the power flow due to finite-heat-capacity may be large enough to prevent temperature profile inversion when the real-fluid term diminishes at cold-end temperatures above about 7 K. Streaming or steady flow also plays a role – flow from the warm end of the regenerator towards the cold end (as is typical in 4 K pulse tube refrigerators) causes profile inversion to occur at lower cold-end temperatures. The azimuthal temperature asymmetry at the cold end (discussed in detail in [5]) appears to occur near the transition from a normal profile to an inverted profile.

Our analytics suggest that for an inverted temperature profile the cold-end cooling power is determined by fluid and material properties at the warm end. For cryocoolers operating above about 7 K, it is therefore more critical to consider power flows at the warm end than at the cold end – perhaps a counterintuitive result. To maximize cooling at the cold end, cryocooler designers may wish to minimize streaming and maximize the heat capacity at the warm end, and cryocooler users may wish to minimize the heat load on the first stage to keep the warm end temperature as low as possible. Furthermore, as we show in another work [4], regenerator cooling is no longer available for regenerators with inverted profiles, so in certain applications it may be critical for designers to ensure that users cannot accidentally push the regenerator into an inverted state.

ACKNOWLEDGMENTS

We thank Vincent Kotsubo of NIST and Gregory Swift of Swift Science and Engineering for discussion and leadership. Contribution of NIST, not subject to copyright. R.S. and S.B. acknowledge support from the Professional Research Experience Program (PREP) between the University of Colorado Boulder and NIST under award number 70NANB18H006. Figures were generated using Matplotlib and fluid properties were gathered using CoolProp [13], an open-source thermophysical library available as a Python wrapper.

REFERENCES

[1] R. Snodgrass, V. Kotsubo, J. Ullom, and S. Backhaus, “Leveraging Real Fluid Effects as a Tool for Power Flow Measurements in 4 K Cryocooler Regenerators,” *Cryocoolers 21*, pp. 315–324, 2021.

[2] N. Rott, “Thermally driven acoustic oscillations, part III: Second-order heat flux,” *Z. Für Angew. Math. Phys. ZAMP*, vol. 26, no. 1, pp. 43–49, Jan. 1975, doi: 10.1007/BF01596277.

[3] G. W. Swift and W. C. Ward, “Simple harmonic analysis of regenerators,” *J. Thermophys. Heat Transf.*, vol. 10, no. 4, pp. 652–662, 1996, doi: 10.2514/3.842.

[4] R. Snodgrass, G. Swift, J. Ullom, and S. Backhaus, “Intermediate cooling from pulse tube refrigerator regenerators operating in the real-fluid regime,” In preparation.

[5] R. Snodgrass, V. Kotsubo, J. Ullom, and S. Backhaus, “A Temperature Instability in 4 K Cryocooler Regenerators Caused by Real Fluid Properties,” *Cryocoolers 21*, pp. 305–313, 2021.

[6] R. Snodgrass, J. Ullom, and S. Backhaus, “Optimal absorption of distributed and conductive heat loads with cryocooler regenerators,” *IOP Conf. Ser. Mater. Sci. Eng.*, vol. 1240, no. 1, p. 012131, 2022, doi: 10.1088/1757-899X/1240/1/012131.

[7] G. W. Swift, *Thermoacoustics: A Unifying Perspective for Some Engines and Refrigerators*, 2nd ed. Springer International Publishing, 2017. doi: 10.1007/978-3-319-66933-5.

[8] B. Ward, J. Clark, and G. Swift, "Users Guide for DeltaEC: Design Environment for Low-amplitude Thermoacoustic Energy Conversion," 2017. www.lanl.gov/thermoacoustics

[9] T. Numazawa, T. Yanagitani, H. Nozawa, Y. Ikeya, R. Li, and T. Satoh, "A New Ceramic Magnetic Regenerator Material for 4 K Cryocoolers," in *Cryocoolers 12*, R. G. Ross, Ed. Boston, MA: Springer US, 2003, pp. 473–481. doi: 10.1007/0-306-47919-2_63.

[10] R. Snodgrass and J. Ullom, "Direct cooling from the regenerators of Gifford-McMahon cryocoolers, with comparison to pulse tube refrigerators," *Cryogenics*, vol. 124, p. 103473, 2022, doi: 10.1016/j.cryogenics.2022.103473.

[11] A. Ravex, T. Trollier, J. Tanchon, and T. Prouvé, "Free Third-Stage Cooling for Two-Stage 4 K Pulse Tube Cryocooler," in *Cryocoolers 14*, 2007, pp. 157–161.

[12] C. Wang, "Extracting Cooling from the Pulse Tube and Regenerator in a 4 K Pulse Tube Cryocooler," in *Cryocoolers 15*, 2009, pp. 177–184.

[13] I. H. Bell, J. Wronski, S. Quoilin, and V. Lemort, "Pure and Pseudo-pure Fluid Thermophysical Property Evaluation and the Open-Source Thermophysical Property Library CoolProp," *Ind. Eng. Chem. Res.*, vol. 53, no. 6, pp. 2498–2508, Feb. 2014, doi: 10.1021/ie4033999.